Mon. Not. R. Astron. Soc. **000**, 1–17 (2007) Printed 3 February 2008 (MN LATEX style file v2.2)

Magnetorotational instability in protoplanetary discs: The effect of dust grains

Raquel Salmeron[1,2] & Mark Wardle[3]
[1] *Planetary Science Institute, Research School of Astronomy & Astrophysics and Research School of Earth Sciences, Australian National University, Canberra ACT 2611, Australia*
[2] *Department of Astronomy & Astrophysics, The University of Chicago, Chicago IL 60637, USA*
[3] *Physics Department, Macquarie University, Sydney NSW 2109, Australia*

2007 March 20

ABSTRACT

We investigate the linear growth and vertical structure of the magnetorotational instability (MRI) in weakly ionised, stratified protoplanetary discs. The magnetic field is initially vertical and dust grains are assumed to be well mixed with the gas over the entire vertical dimension of the disc. For simplicity, all the grains are assumed to have the same radius ($a = 0.1$, 1 or 3 μm) and constitute a constant fraction (1 %) of the total mass of the gas. Solutions are obtained at representative radial locations ($R = 5$ and 10 AU) from the central protostar for a minimum-mass solar nebula model and different choices of the initial magnetic field strength, configuration of the diffusivity tensor and grain sizes.

We find that when no grain are present, or they are $\gtrsim 1$ μm in radius, the midplane of the disc remains magnetically coupled for field strengths up to a few gauss at both radii. In contrast, when a population of small grains ($a = 0.1\mu$m) is mixed with the gas, the section of the disc within two tidal scaleheights from the midplane is magnetically inactive and only magnetic fields weaker than ~ 50 mG can effectively couple to the fluid. At 5 AU, Ohmic diffusion dominates for $z/H \lesssim 1$ when the field is relatively weak ($B \lesssim$ a few milligauss), irrespective of the properties of the grain population. Conversely, at 10 AU this diffusion term is unimportant in all the scenarios studied here. High above the midplane ($z/H \gtrsim 5$), ambipolar diffusion is severe and prevents the field from coupling to the gas for all B. Hall diffusion is dominant for a wide range of field strengths at both radii when dust grains are present.

The growth rate, wavenumber and range of magnetic field strengths for which MRI-unstable modes exist are all drastically diminished when dust grains are present, particularly when they are small ($a \sim 0.1\mu$m). In fact, MRI perturbations grow at 5 AU (10 AU) for $B \lesssim 160$ mG (130 mG) when 3 μm grains are mixed with the gas. This upper limit on the field strength is reduced to only ~ 16 mG (10 mG) when the grain size is reduced to 0.1 μm. In contrast, when the grains are assumed to have settled, MRI unstable modes are found for $B \lesssim 800$ mG at 5 AU and 250 mG at 10 AU (Salmeron & Wardle 2005). Similarly, as the typical size of the dust grains diminishes, the vertical extent of the dead zone increases, as expected. For 0.1 μm grains, the disk is magnetically inactive within two scaleheights of the midplane at both radii, but perturbations grow over the entire section of the disk for grain sizes of 1 μm or larger. When dust grains are mixed with the gas, perturbations that incorporate Hall diffusion grow faster, and are active over a more extended cross section of the disc, than those obtained under the ambipolar diffusion approximation.

We conclude that in protoplanetary discs, the magnetic field is able to couple to the gas and shear over a wide range of fluid conditions even when small dust grains are well mixed with the gas. Despite the low magnetic coupling, MRI modes grow for an extended range of magnetic field strengths and Hall diffusion largely determines the properties of the perturbations in the inner regions of the disc.

Key words: accretion, accretion discs – instabilities – magnetohydrodynamics – stars: formation.

1 INTRODUCTION

Magnetic fields may regulate the 'disc accretion phase' of star formation by providing means of transporting away the excess angular momentum of the disc, enabling matter to accrete. The more generally relevant mechanisms associated with this are MHD turbulence induced by the magnetorotational instability (MRI; Balbus & Hawley 1991, 1998) and outflows driven centrifugally from the disc surfaces (Blandford & Payne 1982, Wardle & Königl 1993; see also the review by Königl & Pudritz 2000). These processes are, in turn, thought to play key roles in the dynamics and evolution of astrophysical accretion discs. Magnetically driven turbulence is likely to impact disc chemistry (e.g. Semenov, Wiebe & Henning 2006, Ilgner & Nelson 2006) as well as the properties – and evolution – of dust grains mixed with the gas (e.g. Turner et al. 2006). Magnetic resonances have been shown to modify the net tidal torque exerted by the disc on a forming planet and thus, alter the speed and direction of the planet's migration through the disc (Terquem 2003; Johnson, Goodman & Menou 2006). Finally, the magnetically inactive (dead) zones (Gammie 1996; Wardle 1997) are not only the regions where planets are thought to form, but they have also been invoked as a possible mechanism to stop their inward migration (e.g. Matsumura & Pudritz 2005).

In protoplanetary discs, however, the magnetic diffusivity can be high enough to limit – or even suppress – these processes. The specific role magnetic fields are able to play in these environments is, therefore, largely determined by the degree of coupling between the field and the neutral gas. A critical parameter for this analysis is the ionisation fraction of the fluid, which reflects the equilibrium between ionisation and recombination processes taking place in the disc. Ionisation processes outside the disc innermost sections ($R \gtrsim 0.1$ AU) are non-thermal, driven by interstellar cosmic rays, X-rays emitted by the magnetically active protostar and radioactive decay (Hayashi 1981; Glassgold, Najita & Igea 1997; Igea & Glassgold 1999; Fromang, Terquem & Balbus 2002). On the other hand, free electrons are lost through recombination processes which, in general, take place both in the gas phase and on grain surfaces (e.g. Nishi, Nakano & Umebayashi 1991).

Dust grains affect the level of magnetic coupling in protoplanetary discs when they are well mixed with the gas (e.g. in relatively early stages of accretion and/or when turbulence prevents them from settling towards the midplane). They do so in two ways. First, they reduce the ionisation fraction by providing additional pathways for electrons and ions to recombine on their surfaces. Second, charged dust particles can become important species in high density regions (Umebayashi & Nakano 1990; Nishi, Nakano & Umebayashi 1991). For example, at 1 AU in a disc where 0.1 μm grains are present, positively charged particles are the most abundant ionised species within two scaleheights from the midplane (see Fig. 6 of Wardle 2007; hereafter W07). As these particles generally have large cross sections, collisions with the neutrals are important and they become decoupled (or partially decoupled) to the magnetic field at densities for which smaller species, typically ions and electrons, would still be well tied to it.

Both of these mechanisms act to lower the conductivity of the fluid, especially near the midplane where the density is high and ionisation processes are inefficient. In the minimum-mass solar nebula disc (Hayashi 1981, Hayashi et el. 1985), for example, X-rays are completely attenuated below $z/H \sim 1.7$ (see Fig. 1 of Salmeron & Wardle 2005; hereafter SW05). As a result, in the disc inner sections the magnetic coupling may be insufficient to provide adequate link between the neutral particles and the field. Moreover, recent calculations for a minimum-mass solar nebula disk exposed to X-ray and cosmic ray ionising fluxes (W07) indicate that near the surface (above 3 - 4 tidal scaleheights) the magnetic diffusivity can also be severe, even though in these regions the ionising flux is strongest and the electron fraction is significantly larger than it is in the disc interior. This effect results from the strong decline in the number density of charged particles high above the midplane. These considerations suggest that magnetic activity in the inner regions of weakly ionised discs may well be confined to intermediate heights above the midplane ($z/H \sim 2-4$).

It is clear that the level of magnetic diffusion is strongly dependent on the presence, and size distribution, of dust particles suspended in the gas phase. In fact, once dust grains have settled, the ionisation fraction may be enough to produce adequate magnetic coupling over the entire vertical extension of the disk even at $R \lesssim 1$ AU (W07). A realistic study of the properties of the MRI in these discs must, therefore, incorporate a consistent treatment of dust dynamics and evolution (unless they are assumed to have settled, a good approximation to model relatively late accretion stages, as was the case in SW03 and SW05). This analysis is further complicated because dust grains have complex spatial and size distributions (e.g. Mathis, Rumpl & Nordsieck 1977, Umebayashi & Nakano 1990, D'Alessio et al. 2006), determined by the competing action of processes involving sticking, shattering, coagulation, growth (and/or sublimation) of ice mantles and settling to the midplane (e.g. Weidenschilling & Cuzzi 1993). Previous results (SW03, SW05) highlight also the importance of incorporating in these studies all three diffusion mechanisms between the magnetic field and the neutral fluid (namely, the Ohmic, Hall and Ambipolar diffusivities), as Hall diffusion largely determines the growth and structure of MRI perturbations, particularly in the disc inner regions (e.g. within distances of the order of a few AU from the central protostar; SW05). This is implemented here via a diffusivity tensor formalism (Cowling 1957, Norman & Heyvaertz 1985, Nakano & Umebayashi 1986, Wardle & Ng 1999, W07).

Dust grains can affect the structure and dynamics of accretion discs via two additional mechanisms: Dust opacity can modify the radiative transfer within the disc – which, in turn, can dramatically alter its structure – and dust particles may become dynamically important if their abundance is sufficiently high. In this study both effects are small because the disc is vertically isothermal and grains constitute only a small fraction of the mass of the gas (see below).

In this paper we study the vertical structure and linear growth of the MRI in a disc where dust grains are well mixed with the gas over its entire vertical dimension. Results are presented for two representative distances ($R = 5$ and 10 AU) from the central protostar. For simplicity, we assume that all particles have the same radius – $a = 0.1$, 1 or 3 μm – and constitute 1% of the total mass of the gas, a typical

assumption in studies of molecular clouds (Umebayashi & Nakano 1990). This fraction is constant with height, which means that we have also assumed that no sedimentation has occurred. Although this is a very simplified picture, the results illustrate the importance of dust particles in the delicate ionisation equilibrium of discs, and consequently, on their magnetic activity.

The paper is organised as follows. The adopted disc model is described in section 2. Section 3 briefly summarises the formulation and methodology, which are based on SW05. We refer the reader to that study – and references therein – for further details. This section also includes a discussion of the typical dependence of the components of the diffusivity tensor and magnetic coupling with height with (and without) grains for the two radial positions of interest. Section 4 then presents the vertical structure and linear growth of unstable MRI modes at these radii and compares solutions incorporating different diffusion mechanisms and assumptions regarding the presence, and size, of dust grains. These results, and possible implications for the dynamics and evolution of low conductivity discs, are discussed in section 5. Our main conclusions are summarised in section 6.

2 DISC MODEL

Our fiducial disc, assumed to be geometrically thin and vertically isothermal, is based on the minimum-mass solar nebula model (Hayashi 1981, Hayashi et al 1985). Our formulation incorporates the disc vertical stratification but – following common practice – it neglects radial gradients. This is appropriate, as these gradients typically occur over a much larger length scale than those in the vertical direction. Under these assumptions, the equilibrium structure of the disc is the result of the balance between the vertical component of the gravitational force exerted by the central object and the pressure gradient within the disc. The vertical profile of the density is then given by

$$\frac{\rho(r,z)}{\rho_0(r)} = \exp\left[-\frac{z^2}{2H^2(r)}\right], \qquad (1)$$

where ρ_0 is the midplane density and $H \equiv c_{\rm s}/\Omega$ is the tidal scaleheight of the gas. The neutral gas is assumed to be composed of molecular hydrogen and helium, such that $n_{\rm He} = 0.2 n_{\rm H_2}$, which results in $n_{\rm H}(r,z) = \rho(r,z)/1.4 m_{\rm H}$.

As already mentioned above, a key feature of protoplanetary accretion discs is that they are weakly ionised. This is because ionisation processes are generally ineffective (except possibly in the vicinity of the star and in the surface regions), while the recombination rate is accelerated by the high density of the fluid and the removal of charges by dust grains (if present). In fact, outside the innermost 0.1 - 0.3 AU, where thermal effects are relevant (e.g. Hayashi 1981), the main ionising sources are X-rays and UV radiation emanating from the central object (e.g. Glassgold, Feigelson & Montmerle 2000) and – to a much lesser extent – the decay of radioactive materials, particularly ^{40}K (Consolmagno & Jokipii 1978, Sano et al. 2000). Interstellar cosmic rays may also be important as they can potentially reach deeper into the disc than X-ray and UV fluxes do. In fact, cosmic rays are the dominant ionising source at 1 AU for $z/H \lesssim 2.2$ (they even reach the midplane at this radius, albeit significantly attenuated; e.g. SW05). However, their actual contribution is unclear because the low-energy particles responsible for ionisation may be scattered by outflows launched from the protostar-disc system (e.g. Fromang et al. 2002). On the other hand, recombination processes in the disc generally occur both in the gas phase (through the dissociative recombination of electrons with molecular ions and the radiative recombination with metal ions) and on grain surfaces (e.g. Oppenheimer & Dalgarno 1974, Spitzer 1978, Umebayashi & Nakano 1980, Nishi et al. 1991, Sano et al. 2000). For a typical abundance of metal atoms in the gas phase of $8.4 \times 10^{-5} \delta_2$[1] (Umebayashi & Nakano 1990), the radiative recombination rate of metal ions is dominant for all vertical locations of interest, with the exception of the uppermost sections of the disc (see Fig. 2 of SW05).

The resulting ionisation fraction of the fluid largely determines the ability of the magnetic field to couple to the gas and shear and thus, regulates the magnetic activity in these astrophysical systems. In protoplanetary discs, in particular, the field has been envisioned to be dynamically important near the surface, whereas magnetic activity may be suppressed in their inner sections (the 'layered accretion' scenario; Gammie 1996, Wardle 1997). However, the existence and configuration of a magnetically inactive – dead – zone in the disk interior has been shown to be critically dependent on the presence and properties of dust grains mixed with the gas (W07). As this study shows, in a minimum-mass solar nebula model at 1 AU the entire cross section of the disc is magnetically coupled when dust grains are assumed to have settled to the midplane. It is, in particular, the presence of small grains what most severely affects the magnetic coupling. For example, the presence of a standard interstellar population of 0.1 μm grains at 1 AU reduces the total active layer of the disc from ~ 1700 g cm^{-2} to ~ 2 g cm^{-2}. This column density increases to ~ 80 g cm^{-2} once the grains aggregate to 3 μm. At 5 AU, in contrast, the entire cross section of the disc is coupled once the grains have grown to 1 μm (we refer the reader to W07 for further details of these models).

3 FORMULATION AND METHODOLOGY

The solutions presented in this paper are based on the formulation detailed in SW03 and SW05. Only a brief summary is given here. We write the equations of non-ideal MHD about a local Keplerian frame that corotates with the disc at the Keplerian frequency Ω and express the velocity field as a departure from exact Keplerian motion. We further assume that the abundances of charged species are sufficiently low to be able to neglect their inertia, thermal pressure and the effect of ionisation and recombination processes on the neutrals. Under these conditions, only the equations of motion for the neutral gas are required:

$$\frac{\partial \rho}{\partial t} + \nabla \cdot (\rho \boldsymbol{v}) = 0\,, \qquad (2)$$

[1] Here $\delta_2 \approx 0.02$ is the fraction of heavy metal atoms in the gas phase, estimated from interstellar absorption lines in diffuse clouds (Morton 1974).

$$\frac{\partial \boldsymbol{v}}{\partial t}+(\boldsymbol{v}\cdot\nabla)\boldsymbol{v}-2\Omega v_\phi\hat{\boldsymbol{r}}+\tfrac{1}{2}\Omega v_r\hat{\boldsymbol{\phi}}-\frac{v_K^2}{r}\hat{\boldsymbol{r}}+\frac{c_s^2}{\rho}\nabla\rho+\nabla\Phi=\frac{\boldsymbol{J}\times\boldsymbol{B}}{c\rho}\,, \tag{3}$$

$$\frac{\partial \boldsymbol{B}}{\partial t}=\nabla\times(\boldsymbol{v}\times\boldsymbol{B})-c\nabla\times\boldsymbol{E}'-\tfrac{3}{2}\Omega\boldsymbol{B}_r\hat{\boldsymbol{\phi}}\,. \tag{4}$$

In the equation of motion (3), Φ is the gravitational potential for a non self-gravitating disc and $\boldsymbol{v}_{\rm K}^2/r$ is the centripetal term generated by Keplerian motion. Coriolis terms $2\Omega v_\phi\hat{\boldsymbol{r}}$ and $\frac{1}{2}\Omega v_r\hat{\boldsymbol{\phi}}$ are associated with the use of a local Keplerian frame and $c_{\rm s}$ is the isothermal sound speed. In the induction equation (4), $\boldsymbol{E}'$ is the electric field in the frame comoving with the neutrals and $\frac{3}{2}\Omega\boldsymbol{B}_r\hat{\boldsymbol{\phi}}$ accounts for the generation of toroidal field by the disc differential rotation. Finally, the magnetic field must also satisfy the constraint $\nabla\cdot\boldsymbol{B}=0$ and the current density must satisfy Ampere's law,

$$\boldsymbol{J}=\frac{c}{4\pi}\nabla\times\boldsymbol{B} \tag{5}$$

and Ohm's law

$$\boldsymbol{J}=\boldsymbol{\sigma}\cdot\boldsymbol{E}'\,. \tag{6}$$

Following Wardle & Ng (1999) and Wardle (1999; hereafter W99), the current density is expressed as,

$$\boldsymbol{J}=\boldsymbol{\sigma}\cdot\boldsymbol{E}'=\sigma_{\rm O}\boldsymbol{E}'_\parallel+\sigma_{\rm H}\hat{\boldsymbol{B}}\times\boldsymbol{E}'_\perp+\sigma_{\rm P}\boldsymbol{E}'_\perp\,, \tag{7}$$

where subscripts $\parallel$ and $\perp$ denote vector components parallel and perpendicular to $\mathbf{B}$. In this expression, $\sigma_{\rm O}$, $\sigma_{\rm H}$ and $\sigma_{\rm P}$ are the Ohmic, Hall and Pedersen conductivity terms given by,

$$\sigma_{\rm O}=\frac{ec}{B}\sum_j n_jZ_j\beta_j\,, \tag{8}$$

$$\sigma_{\rm H}=\frac{ec}{B}\sum_j\frac{n_jZ_j}{1+\beta_j^2} \tag{9}$$

and

$$\sigma_{\rm P}=\frac{ec}{B}\sum_j\frac{n_jZ_j\beta_j}{1+\beta_j^2}\,. \tag{10}$$

Subscript j is used here to label the charged species. They are characterised by their number density n_j, particle mass m_j, charge Z_je and Hall parameter

$$\beta_j=\frac{Z_jeB}{m_jc}\,\frac{1}{\gamma_j\rho} \tag{11}$$

(the ratio of the gyrofrequency and the collision frequency with the neutrals), which measures the relative importance of the Lorentz and drag forces in balancing the electric force on the particle.

Equation (7) can be inverted to find an expression for $\boldsymbol{E}'$. This leads to the following form of the induction equation (W07)

$$\frac{\partial \boldsymbol{B}}{\partial t}=\nabla\times(\boldsymbol{v}\times\boldsymbol{B})-\nabla\times\Big[\eta_{\rm O}\nabla\times\boldsymbol{B}+\eta_{\rm H}(\nabla\times\boldsymbol{B})\times\hat{\boldsymbol{B}}+\eta_{\rm A}(\nabla\times\boldsymbol{B})_\perp\Big]\,, \tag{12}$$

where

$$\eta_{\rm O}=\frac{c^2}{4\pi\sigma_{\rm O}}\,, \tag{13}$$

$$\eta_{\rm H}=\frac{c^2}{4\pi\sigma_\perp}\frac{\sigma_{\rm H}}{\sigma_\perp} \tag{14}$$

and

$$\eta_{\rm A}=\frac{c^2}{4\pi\sigma_\perp}\frac{\sigma_{\rm P}}{\sigma_\perp}-\eta_{\rm O} \tag{15}$$

are the Ohmic, Hall and ambipolar diffusivities; and

$$\sigma_\perp=\sqrt{\sigma_{\rm H}^2+\sigma_{\rm P}^2} \tag{16}$$

is the total conductivity perpendicular to the magnetic field. When ions and electrons are the only charged species, it can be shown that (W07)

$$|\eta_{\rm H}|=|\beta_{\rm e}|\eta_{\rm O} \tag{17}$$

and

$$\eta_{\rm A}=|\beta_{\rm e}|\beta_{\rm i}\eta_{\rm O}\,. \tag{18}$$

Note that the Ohmic ($\eta_{\rm O}$) and ambipolar ($\eta_{\rm A}$) diffusivity terms are always positive, as the former does not depend on the magnetic field strength and the second scale quadratically with it. As a result, they are both invariant under a reversal of the magnetic field polarity. On the contrary, the Hall term ($\eta_{\rm H}$) scales linearly with B and thus, can become negative. The change in sign of $\eta_{\rm H}$ corresponds, in turn, to a change in the direction of the magnetic field at the height where particular species become decoupled to it by collisions with the neutrals. It corresponds, therefore, to changes in the contribution of different charged species to this component of the diffusivity tensor.

The relative importance of the diffusion terms in (13) to (15) differentiate three *diffusivity regimes*:

(i) In the *Ambipolar diffusion* regime, $|\beta_j|\gg1$ for most charged species and $\eta_{\rm A}\gg|\eta_{\rm H}|\gg\eta_{\rm O}$. In this limit, which is typically dominant in low density regions (e.g. in molecular clouds and near the surface of protoplanetary discs), the magnetic field is effectively frozen into the ionized component of the fluid and drifts with it through the neutrals.

(ii) *Ohmic (resistive)* limit. In this case $|\beta_j|\ll1$ for most charged species, resulting in $\eta_{\rm O}\gg|\eta_{\rm H}|\gg\eta_{\rm A}$. The magnetic field can not be regarded as being frozen into any fluid component and the diffusivity is a scalar, the well-known Ohmic diffusivity. This regime dominates close to the midplane in the inner regions ($R\lesssim5$ AU) of protoplanetary discs when the magnetic field is relatively weak (W07).

(iii) *Hall diffusion* limit, which occurs when $|\beta_j| \gg 1$ for charged species of one sign (typically electrons) and $\ll 1$ for those of the other sign (e.g. ions). In this case, $|\eta_{\rm H}| \gg \eta_{\rm A}$ and $\eta_{\rm O}$. This regime is important at intermediate densities (between those at which ambipolar and Ohmic diffusion regimes dominate). It has been shown to prevail under fluid conditions satisfied over vast regions in protoplanetary discs (e.g. Sano & Stone 2002a, W07).

The diffusivities used in this study were calculated using the procedure described in W07, to which we refer the reader for details. Essentially, the adopted chemical reaction scheme is based on that of Nishi, Nakano & Umebayashi (1991), but it allows for higher charge states on dust grains. This is necessary because of the higher temperature and density of protoplanetary discs in relation to those typically associated with molecular clouds.

Finally, in the following sections we will also use the magnetic coupling parameter (W99)

$$\chi \equiv \frac{\omega_{\rm c}}{\Omega} = \frac{1}{\Omega}\frac{B_0\sigma_\perp}{\rho c^2}\,, \tag{19}$$

the ratio of the critical frequency ($\omega_{\rm c}$) *above* which flux-freezing conditions break down and the dynamical (Keplerian) frequency of the disc. For the sake of clarity we now sketch the arguments leading to this expression (see also Wardle & Ng 1999). First, recall that non-ideal MHD effects become important when the inductive and diffusive terms in the induction equation (4) are comparable; or

$$\nabla \times (\boldsymbol{v} \times \boldsymbol{B}) \sim c\nabla \times \boldsymbol{E}'\,, \tag{20}$$

where (see equation 6)

$$\boldsymbol{E}' = \frac{\boldsymbol{J}}{\sigma} = \frac{1}{\sigma}\left(\frac{c}{4\pi}\nabla \times \boldsymbol{B}\right)\,. \tag{21}$$

In expression (21), σ is taken to be a characteristic measure of the conductivity of the gas. Next, we adopt the following typical values for the various terms above

$$\nabla \sim k = \omega/v_{\rm A} \qquad v \sim v_{\rm A} \qquad B \sim B_0 \qquad \sigma \sim \sigma_\perp\,,$$

where k is the wavenumber of the MRI perturbations in flux-freezing conditions and $v_{\rm A} \equiv B^2/4\pi\rho$ is the local Alfvén speed. Substituting these relations in (20) yields the desired expression for $\omega_{\rm c}$. This parameter is useful because in ideal-MHD conditions, the instability grows at $\sim 0.75\Omega$ (Balbus & Hawley 1991). Consequently, if $\omega_{\rm c} < \Omega$ (or $\chi < 1$) the field is poorly coupled to the disc at the frequencies of interest for the analysis of the MRI and non-ideal MHD effects are expected to be important.

Equations (2) to (5) and (7) are linearized about an initial (labeled by a subscript '0'), steady state where the magnetic field is vertical and the current density, fluid velocity and electric field in the frame comoving with the neutrals all vanish. As a result of the last condition, the changes in the components of the diffusivity tensor are not relevant in this linear formulation (e.g. $\boldsymbol{E}_0' \cdot \delta\boldsymbol{\sigma} \equiv 0$) and only the initial, unperturbed values are required. Taking perturbations of the form $\mathbf{q} = \mathbf{q}_0 + \delta\mathbf{q}(z)e^{i\omega t}$ and assuming $k = k_z$ we obtain a system of ordinary differential equations (ODE) in $\boldsymbol{\delta E}$ (the perturbations of the electric field in the laboratory frame), $\boldsymbol{\delta B}$, and the perturbations' growth rate $\nu = i\omega/\Omega$. Three parameters are found to control the dynamics and evolution of the fluid: (1) $v_{\rm A}/c_{\rm s}$, the local ratio of the Alfvén speed and the isothermal sound speed of the gas, which measures the strength of the magnetic field. (2) χ, the coupling between the ionised and neutral components of the fluid. (3) $\eta_{\rm H}/\eta_{\rm P}$, the ratio of the diffusivity terms perpendicular to $\mathbf{B}$, which characterises the diffusivity regime of the fluid. These parameters are evaluated at different locations (r, z) of the disc taking the magnetic field strength ($B > 1$ mG) as a free parameter. The system of equations is integrated vertically as a two-point boundary value problem for coupled ODE with boundary conditions $\delta B_r = \delta B_\phi = 0$ and $\delta E_r = 1$ at $z = 0$ and $\delta B_r = \delta B_\phi = 0$ at $z/H = 6$.

Given that magnetic diffusion can have such a dramatic effect on the properties of magnetically-driven turbulence in protoplanetary discs, we now present calculations of the magnetic diffusivity at 5 and 10 AU. We explore which disc regions are expected to be magnetically coupled and which diffusion mechanism is dominant at different positions (r, z) as a function of B. This discussion is relevant for the analysis of our MRI results at these locations (section 4).

3.1 Magnetic diffusivity

Fig. 1 shows the components of the diffusivity tensor ($\eta_{\rm O}$, $|\eta_{\rm H}|$ and $\eta_{\rm A}$) as a function of height for $R = 10$ AU and a representative field strength ($B = 10$ mG). The solutions in the top panel have been obtained assuming that dust grains have settled into a thin layer about the midplane, so the charges are carried by ions and electrons only. The results in the middle and bottom panels incorporate a population of 1 and 0.1 μm-sized grains, respectively. Note that when dust grains are present, all diffusivity terms increase drastically in relation to their values in the no-grains scenario. This effect becomes more accentuated as the grain size diminishes, given the efficiency of small grains in removing free electrons from the gas. For example, in the case that incorporates 0.1 μm-sized particles (bottom panel), the diffusivity components at the midplane are larger, by 4 – 7 orders of magnitude, than their corresponding values when the grains have settled.

When dust grains have either settled or aggregated to at least 1 μm in size (see top and middle panels), $|\eta_{\rm H}|$ is dominant for $z/H \lesssim 2.5$ and the fluid in this region is in the Hall diffusivity regime. Also, $\eta_{\rm A} > \eta_{\rm O}$ there which implies that, if ions and electrons are the sole charge carriers, $|\beta_{\rm e}|\beta_{\rm i} > 1$ (see equation 18). For higher z, $\eta_{\rm A} > |\eta_{\rm H}| > \eta_{\rm O}$ and ambipolar diffusion dominates. Note that the Hall diffusivity term increases less sharply than the ambipolar diffusivity in response to the fall in fluid density. This is a general feature, and an expected one, given that the former scales with ρ^{-1} and the latter with ρ^{-2}. As a result, $\eta_{\rm A}$ is typically several orders of magnitude larger than $|\eta_{\rm H}|$ near the surface regions of the disc. Finally, for the 0.1 μm-sized grain population (bottom panel), $\eta_{\rm A} > |\eta_{\rm H}|$ for all z. This can be traced back to the fact that Hall diffusion is suppressed here because of the nearly equal abundances of (negatively charged) grains and ions in this region.

Note also that the Hall diffusivity component shows characteristic 'spikes', at the heights where it changes sign.

This effect is also particularly evident for the 0.1 μm-sized grains. In this scenario, in particular, $\eta_{\rm H}$ is positive when $0 \lesssim z/H \lesssim 1.6$ and $2.5 \lesssim z/H \lesssim 4.1$. It is negative at all other vertical locations. As mentioned above, this corresponds to different charged species contributing to this diffusion term. In order to explore the contributions to $\eta_{\rm H}$ in each of the vertical sections in which it has a different sign, we now describe the behaviour of the charged species at four representative heights, namely $z/H = 1$ and 3 (for which $\eta_{\rm H} > 0$), and $z/H = 2$ and 5 (where $\eta_{\rm H} < 0$).

At $z/H = 1$, the density is sufficiently high for electrons to be able to stick to the grains. As a result, they reside mainly on dust particles, as do about a third of the ions. The contribution of (negatively charged) grains and ions to the Hall diffusivity term are very similar, with a small positive excess, which determines the sign of $\eta_{\rm H}$ in this region. On the contrary, at $z/H = 2$, ions are the dominant positively charged species, while the negative charges are still contained in dust grains and drift together with the neutrals. Consequently, $\eta_{\rm H}$ is negative in this section of the disc. At $z/H = 3$, ions and electrons are the main charge carriers and ions dominate the contribution to the Hall term, which makes $\eta_{\rm H}$ positive. Finally, for $z/H = 5$, the dominant contribution to the Hall diffusivity term comes from the small percentage of remaining negatively charged grains. As a result, $\eta_{\rm H}$ is negative (and very small).

We now turn our attention to $R = 5$ AU (Fig. 2). At this radius, when the dust particles are at least 1 μm in size (or are absent), Hall diffusion dominates for $z/H \lesssim 3$. In contrast with the solutions at 10 AU, however, Ohmic diffusion dominates over ambipolar diffusion ($\eta_{\rm O} > \eta_{\rm A}$) for most of this region (which implies that $|\beta_{\rm e}|\beta_{\rm i} < 1$ in this section of the disc when no grains are present). This is expected, given the larger fluid density at this radius in comparison with the 10 AU case discussed above. When the grains are small ($a = 0.1$ μm, see bottom panel), ambipolar diffusion is dominant ($\eta_{\rm A} > |\eta_{\rm H}| > \eta_{\rm O}$) for $1 \lesssim z/H \lesssim 2.8$ and $z/H \gtrsim 3.5$. At all other heights, $\eta_{\rm A} \approx |\eta_{\rm H}| > \eta_{\rm O}$.

Figs. 3 and 4 generalise the analysis of the previous paragraphs to other field strengths for $R = 10$ and 5 AU, respectively. As before, the top panels refer to discs where no grains are present. The middle and bottom panels incorporate 1 and 0.1 μm-sized grains, respectively. In these plots, the contours show the values of $\tilde{\eta} \equiv (\eta_{\rm O}^2 + \eta_{\rm H}^2 + \eta_{\rm A}^2)^{1/2}$ and the background shading (from dark to light) denotes the dominant diffusion mechanism as Ohmic, Hall or Ambipolar. The solid line is the critical value of the diffusivity $\tilde{\eta}_{\rm crit} \equiv H c_{\rm s}$ (W07), above which the diffusion term in the induction equation $|\nabla \times (\tilde{\eta} \nabla \times \boldsymbol{B})|$is larger than the inductive term $|\nabla \times (\boldsymbol{v} \times \boldsymbol{B})|$(see equation 4), a situation that effectively limits the ability of the field to couple to the Keplerian shear. The dashed lines correspond to increases (decreases) in $\tilde{\eta}$ by factors of 10 in the direction of a stronger (weaker) magnetic field.

Note that at 10 AU, in the no-grains case (top panel of Fig. 3), field strengths $\lesssim$ a few Gauss are able to couple to the gas at the midplane. Hall diffusion dominates at this location for $B \lesssim 0.1$ G but the range of field strengths over which this occurs decreases gradually with height, so that when $z/H \gtrsim 3.3$ ambipolar diffusion is dominant for all B. The coupled region potentially extends to $z/H \sim 4.5$, depending on the field strength. When the particles have aggregated to 1 μm in size (middle panel of Fig. 3), the situation is qualitatively similar to the one just discussed, the only significant difference being that in this case Hall diffusion is dominant at the midplane for all B that can couple to the gas.

The previous results, however, are significantly modified when small dust grains are present ($a = 0.1$ μm, bottom panel). In this case, the section of the disc below two scaleheights is magnetically inactive and the magnetic diffusivity is severe enough to prevent coupling over the entire disc thickness when $B \gtrsim 25$ mG. Ambipolar diffusion dominates for all field strengths above $\sim$ four scaleheights and also for ~ 1 mG $\lesssim B \lesssim 10 - 100$ mG below this height (the actual upper limit of this range varies with z). Hall diffusion is inhibited close to the midplane for this range of field strengths because the number density of positively and negatively charged grains are very similar. Note, finally, that Ohmic diffusion is not dominant in any of the depicted scenarios at this radius, as expected, given the relatively low density of the fluid.

The results at 5 AU are qualitatively similar (Fig. 4) to the ones just discussed. One key difference, however, is that Ohmic diffusion dominates in all cases for $z/H \lesssim 1.2$ provided that the field is sufficiently weak ($B \lesssim$ a few milligauss). Ambipolar diffusion, on the other hand, is dominant for relatively strong fields (e.g. $B \gtrsim 1$ G at $z = 0$ in the no-grains case) as well as for all B near the disk surface ($z/H \gtrsim 4$). Hall diffusivity is the most important diffusion mechanism for fluid conditions in-between those specified above. Note that the coupled region extends up to $z/H \sim 5$ in all cases. When no grains are present (top panel) the midplane is coupled for fields up to a few Gauss. This upper limit drops to ~ 20 mG when 1 μm grains are mixed with the gas. When the grains are 0.1 μm in size, however, only the region above $z/H \sim 2.5$ is coupled, and only for $B \lesssim 50$ mG. This 'dead' zone is slightly more extended at this radius than at 10 AU, but stronger fields are able to couple to the gas in this case. The steep contours close to the midplane in this scenario result from the pronounced increase in the diffusivity in response to the increase in fluid density and the decline in the ionisation fraction of the gas as z diminishes.

3.2 Magnetic coupling and MRI unstable modes

In this section we address the following question: Which magnetic diffusion mechanism determines the properties of the MRI in different regions in protoplanetary discs? In this connection, it is useful to recall (see W99, SW03 and references therein for details) that in the disc regions where the magnetic coupling $\chi > 10$, ideal-MHD conditions hold and the particular configuration of the diffusivity tensor has little effect on the behaviour of the MRI. When χ is weaker than this but $\gtrsim |\sigma_{\rm H}|/\sigma_{\perp}$, ambipolar diffusion dominates. Finally, in the regions where $\chi < |\sigma_{\rm H}|/\sigma_{\perp}$, Hall diffusion modifies the structure and growth of MRI unstable modes, provided that this degree of coupling is sufficient for unstable modes to grow.

Figs. 5 and 6 compare χ with the ratio $|\sigma_{\rm H}|/\sigma_{\perp}$ at $R = 10$ and 5 AU, respectively, as a function of the magnetic field strength and for different assumptions regarding the presence, and radius, of dust grains mixed with the gas. In each figure, the top panels depict the results obtained

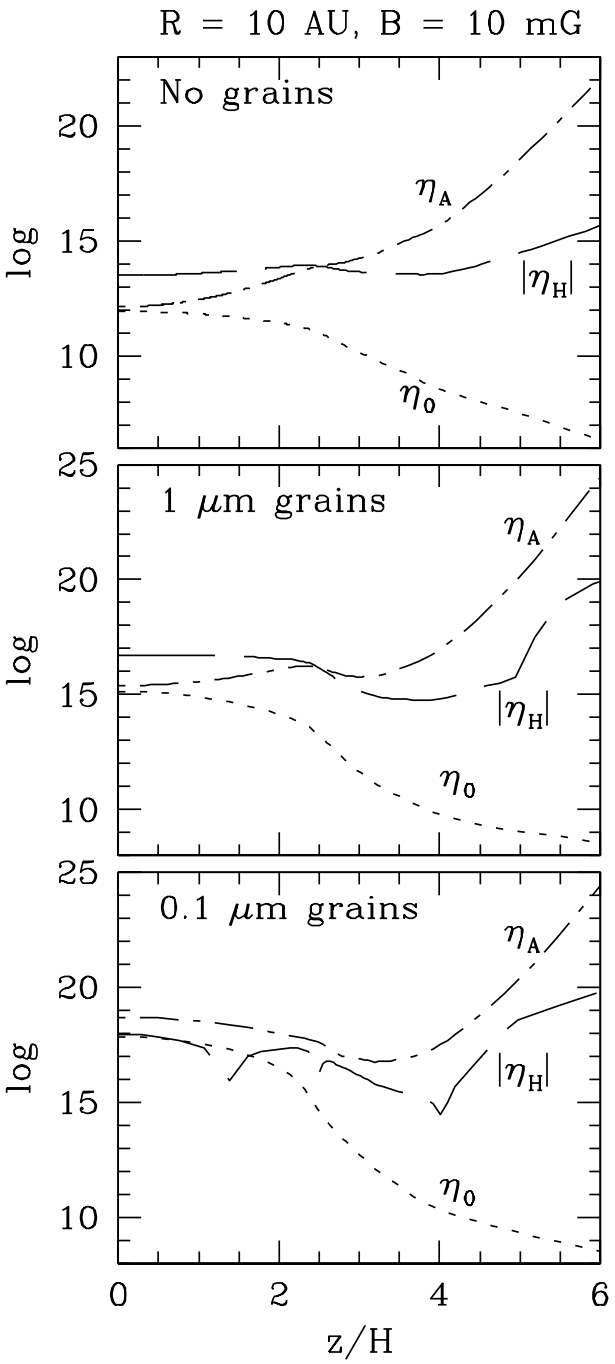

Figure 1. Components of the diffusivity tensor (η_O, $|\eta_H|$ and η_A) as a function of height for $R = 10$ AU and $B = 10$ mG. In the top panel, dust grains have settled to the midplane. The middle and bottom panels show the solutions when dust grains of radius $a = 1$ and 0.1 μm, respectively, are well mixed with the gas over the entire disc thickness. When the grains are $\gtrsim 1$ μm in size (or are absent), Hall diffusion dominates for $z/H \lesssim 2.5$. In contrast, for the 0.1 μm-sized grains, $\eta_A > |\eta_H|$ for all z and $|\eta_H| > \eta_O$ above $z/H \sim 1$. Note that $|\eta_H|$ shows 'spikes' at the z where it changes sign in response to different charged species becoming decoupled to the magnetic field by collisions with the neutrals.

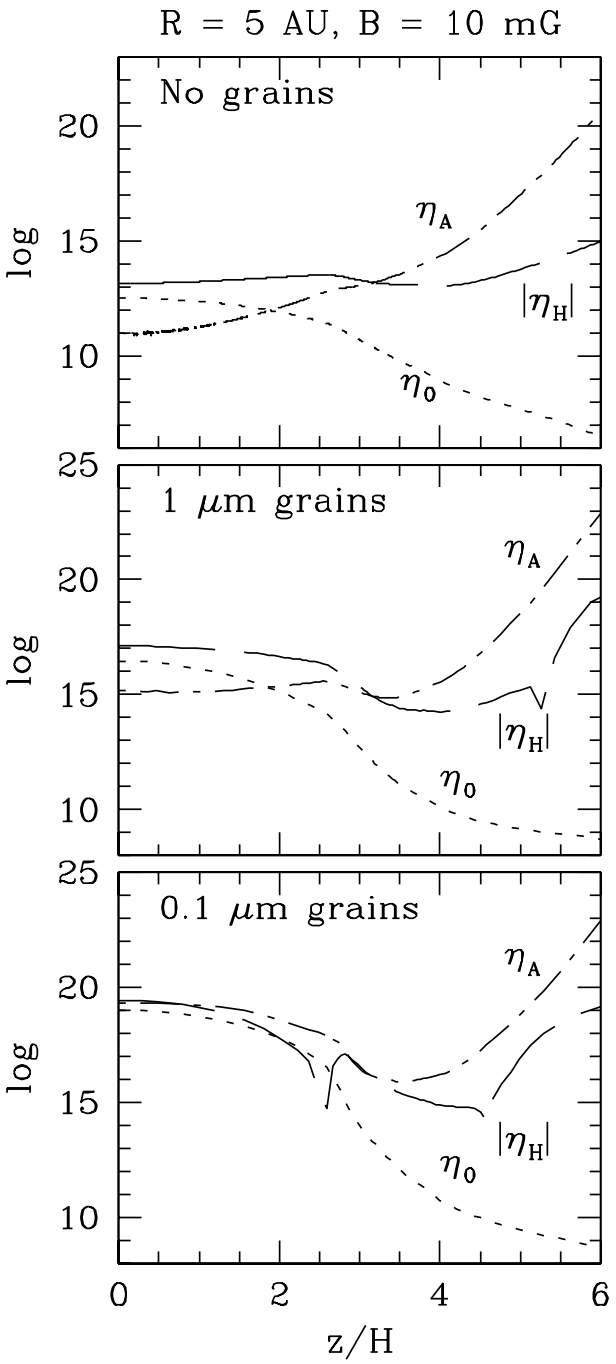

Figure 2. As per Fig. 1 for R = 5 AU. Note that when the grains are $\gtrsim 1\mu$m in size or are absent (top and middle panels), Hall diffusion dominates for $z/H \lesssim 3$. At this radius, however, $\eta_O > \eta_A$ for $z/H \lesssim 2$.

assuming that no grains are present whereas the effect of 1 μm (0.1 μm)-sized grains is shown in the middle (bottom) panels. Note the dramatic impact dust grains have in the level of magnetic coupling at both radii. For example, introducing a population of 0.1 μm grains causes χ to drop by 6 - 8 orders of magnitude at the midplane. Bottom (solid) and leftmost (dashed) lines correspond to $B = 1$ mG in all cases. The field strength increases by a factor of ten towards larger χ, except that at both radii the top (and rightmost)

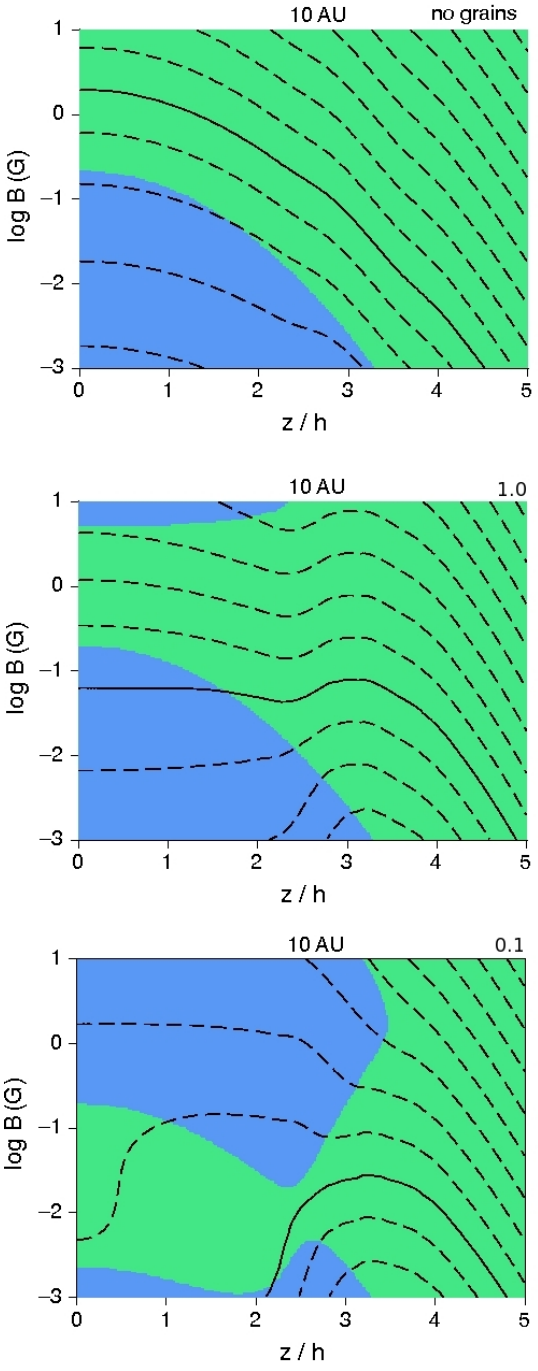

Figure 3. Contours of $\tilde{\eta} \equiv (\eta_{\rm O}^2 + \eta_{\rm H}^2 + \eta_{\rm A}^2)^{1/2}$ in a log(B) - z/H plane for $R = 10$ AU. In the top panel, dust particles are assumed to have settled to the midplane. The effect of dust grains is included in the middle ($a = 1$ μm) and bottom ($a = 0.1$ μm) panels. The solid line is the critical value of the diffusivity $\tilde{\eta}_{\rm crit} \equiv Hc_{\rm s}$ (W07) above which the magnetic field does not couple to the gas and shear. The background shading (from dark to light) denotes the dominant diffusion mechanism as Ohmic, Hall or Ambipolar. Note that when the grain size is 1 μm or larger (or they have settled), the disc midplane is magnetically coupled for a range of B. In contrast, when the grains are small (bottom panel), magnetic diffusion prevents the field to couple to the gas for $z/H \lesssim 2$.

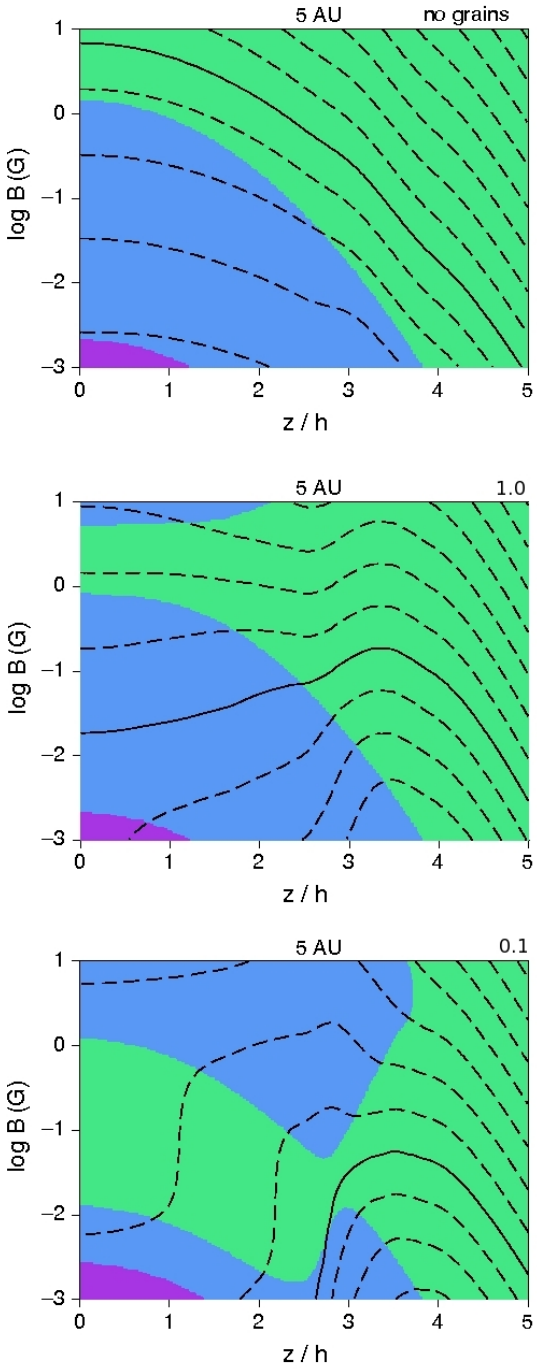

Figure 4. As per Fig. 3 for $R = 5$ AU. Note that in all cases, Ohmic diffusion is dominant close to the midplane ($z/H \lesssim 1.2$) when the field is weak ($B <$ a few mG). The midplane can be magnetically coupled when the grains are absent or have aggregated to $a \gtrsim 1$ μm. However, a dead zone develops below ~ 2.5 scaleheights when they are small ($a = 0.1$ μm). In this scenario, only $B \lesssim 50$ mG can couple to the gas (and only for $z/H \gtrsim 2.5$). Note that ambipolar diffusion dominates for all B when $z/H \gtrsim 4$ (all panels) and for 1 mG $\lesssim B \lesssim 10 - 100$ mG below this height (bottom panel only).

curves for $a = 1$ μm show the maximum field strength for which the MRI grows. This is also the case for the solutions with no grains at 5 AU (the maximum values of B for these cases are noted in the captions of Figs. 5 and 6).

Note that at 10 AU (Fig. 5), Hall diffusion is not expected to play an important role in the local properties of the MRI once the grains have settled ($\chi > |\sigma_{\rm H}|/\sigma_{\perp}$ for all z and B). In this scenario, ambipolar diffusion dominates in the inner sections of the disc when the field is weak ($z/H \lesssim 2$ and $B \lesssim 10$ mG) while ideal-MHD holds at all heights for stronger B. On the contrary, when either 1 or 0.1 μm grains are mixed with the gas (middle and bottom panels), Hall diffusion has an impact on the MRI within $\sim$ three scaleheights of the midplane. At higher z, the ionisation fraction is such that $|\sigma_{\rm H}|/\sigma_{\perp} \lesssim \chi \lesssim 10$ and ambipolar diffusion determines the local properties of MRI unstable modes.

The corresponding solutions at 5 AU are shown in Fig. 6. In this case, Hall diffusion dominates within two scaleheights from the midplane if the magnetic field is weak ($B \lesssim 10$ mG) and the grains have settled (top panel). This is consistent with the higher column density at this radius in comparison to the 10 AU case discussed above (for which Hall diffusion was unimportant). Ambipolar diffusion is dominant in this scenario for 10 mG $\lesssim B \lesssim$ 100 mG but for stronger fields, $\chi > 10$ for all z and the fluid is in ideal-MHD conditions over the entire section of the disc. On the other hand, when dust grains are present (middle and bottom panels), Hall diffusion determines the properties of MRI-unstable modes in the inner sections of the disc ($z/H \lesssim 3$) for all magnetic field strengths for which they grow. Ambipolar diffusion is locally dominant at higher z.

Finally, note that when dust grains are present, the extent of the disc section where Hall diffusion has an impact on the MRI at both radii is quite insensitive to the strength of the field. Evidently, dust particles can efficiently reduce the degree of magnetic coupling in the disc inner sections for a wide range of magnetic field strengths. In light of the concepts presented so far, we now analyse the properties of the MRI at the two radii of interest.

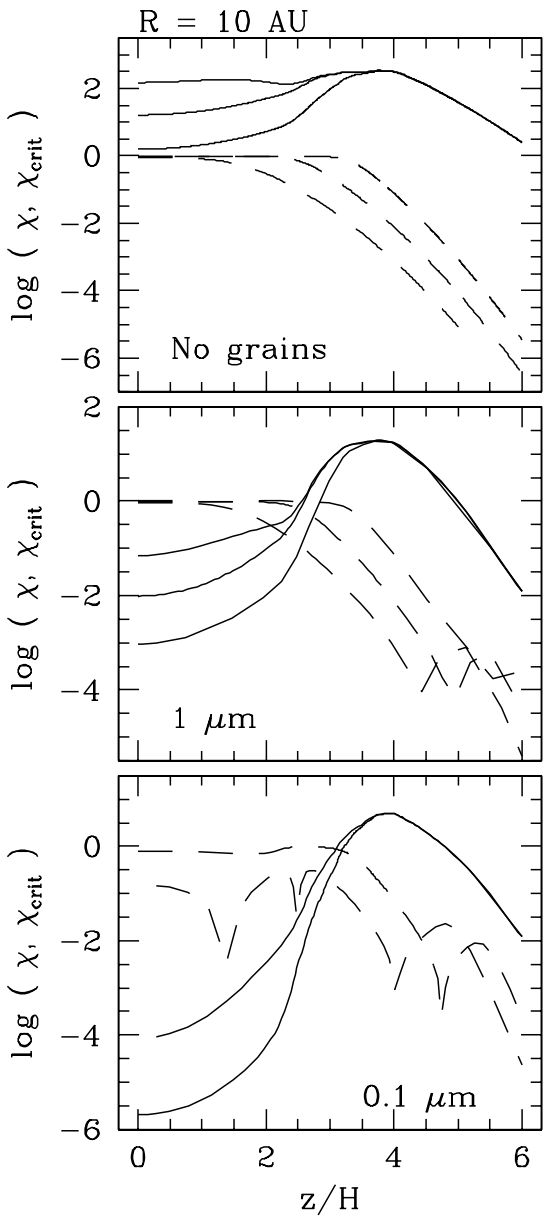

Figure 5. Comparison of the local magnetic coupling χ (solid lines) and critical coupling $\chi_{\rm crit} \equiv |\sigma_{\rm H}|/\sigma_{\perp}$ (dashed lines) for $R = 10$ AU as a function of the magnetic field strength and for different assumptions regarding the presence (and size) of dust grains. Hall diffusion modifies the structure and growth rate of MRI unstable modes in the regions where $\chi < \chi_{\rm crit}$ provided that the coupling is sufficient for the instability to operate (SW03). Ambipolar diffusion is important if $\chi_{\rm crit} < \chi \lesssim 10$. For stronger χ, ideal-MHD describes the fluid adequately (W99). The bottom (and leftmost) lines correspond to $B = 1$ mG in all panels. B increases by a factor of 10 between curves (towards larger χ), except that the top curve for $a = 1$ μm grains corresponds to $B = 77$ mG, the strongest field for which perturbations grow.

4 MAGNETOROTATIONAL INSTABILITY

Figs. 7 and 8 compare the vertical structure and growth rate of the most unstable MRI modes at $R = 10$ and 5 AU, respectively, for different choices of the magnetic field strength. The left column of each figure displays solutions obtained assuming that grains have settled out of the gas phase. The remaining columns – from left to right – show results that incorporate the effect of a different population of single- sized dust particles of radius $a = 3$, 1 and 0.1 μm, respectively. Note how the growth rate, wavenumber and range of magnetic field strengths for which unstable modes exist are all drastically diminished when dust grains are present. This is expected, given the reduction in the coupling between the neutral and ionised components of the fluid when dust grains (particularly if they are small) are well mixed with the gas. Note also that the range of field strengths for which unstable modes are found matches quite well with the range for which the magnetic field is expected to couple to the fluid, as discussed in section 3.1 (see Figs. 3 and 4 and compare the maximum magnetic field strength for which the MRI grows and the maximum B that can couple to the gas at the z where the modes peak).

For the discussion that follows, it is useful to keep in mind that both the growth rate and the envelope of these perturbations are shaped by the interplay of different diffusion mechanisms, whose relative importance vary strongly

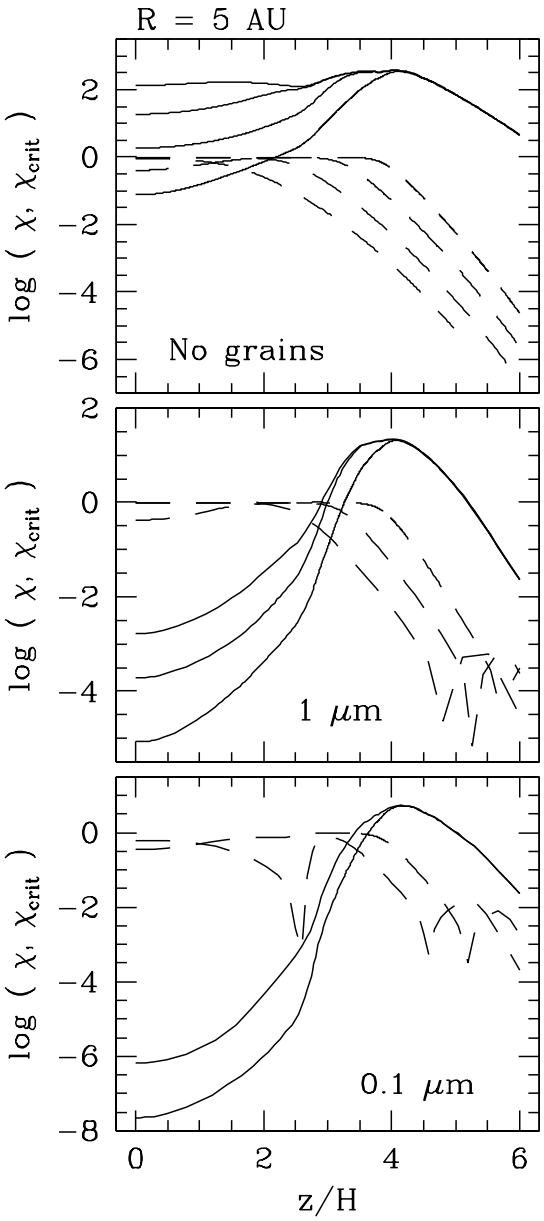

Figure 6. As per Fig. 5 for $R = 5$ AU. Note, however, that the top (and rightmost) lines correspond to $B = 795$ mG (top panel) and $B = 83$ mG (middle panel), the maximum field strength for which unstable modes grow in each scenario.

with height. In particular, the ambipolar diffusion component of the diffusivity tensor drives the local growth rate (and thus the amplitude of global perturbations) to increase with z (SW03). This is because, in this diffusion regime, the maximum growth rate increases with the local χ (W99) and is, therefore, a strong function of the vertical location. Accordingly, the envelopes of the perturbations driven by this term typically peak at an intermediate height above the midplane. On the contrary, the maximum growth rate of Hall perturbations is insensitive to χ (W99). Because they are not driven from any particular vertical location, their envelope is fairly flat (SW03). We now analyse the structure and growth of the perturbations at the two radii of interest. The properties of these modes without dust grains were discussed in detail in SW05. For the sake of clarity, these results are briefly summarised as part of this discussion.

At 10 AU, ambipolar diffusion drives the MRI when the field is weak ($B \lesssim 10$ mG) and ions and electrons are the sole charge carriers (see top panel of Fig. 5). As a result, unstable modes peak above the midplane in this scenario (left column of Fig. 7; e.g. the mode computed with $B = 1$ mG peaks at $z/H \sim 0.5$). For stronger fields, ideal-MHD holds at all z. This explains the flat envelope, and fast growth, of the perturbations obtained with $B = 10$ and 100 mG. Unstable modes are found in this case for $B \lesssim 250$ mG and they grow at about the ideal-MHD rate for 2 mG $\lesssim B \lesssim 50$ mG. When B is even stronger than 250 mG, the wavelength of the most unstable mode is $\sim H$, the disc tidal scaleheight, and the perturbations are strongly damped (Balbus & Hawley 1991). Finally, note that no dead zone develops in this scenario, given that the magnetic field is coupled to the gas even at the midplane (see top panel of Fig. 3).

We now turn our attention to the solutions obtained under the assumption that dust grains are present at this radius. Note that when the dust particles are relatively large ($a = 3$ and 1 μm, central two columns of Fig. 7), the perturbations exhibit the flat envelope that is typical when Hall diffusion controls their behaviour (for these fluid conditions Hall diffusion is expected to modify MRI modes for $z/H \lesssim 2.5$, Fig. 5). These modes grow even at the midplane, a result consistent with the level of magnetic coupling associated with this disc model (e.g. see middle panel of Fig. 3). On the other hand, when the dust grains are small (rightmost column of Fig. 7) the low magnetic coupling, especially within two scaleheights of the midplane (Fig. 3, bottom panel), causes the amplitude of all perturbations in this section of the disc to be severely reduced. Unstable modes were found here only for $B \lesssim 10$ mG, a much reduced range compared with the $B \approx 250$ mG for which they exist when ions and electrons are the only charge carriers.

Fig. 8 shows the solutions obtained for $R = 5$ AU. At this radius, MRI unstable modes grow – without grains – for $B \lesssim 795$ mG. Moreover, they grow at essentially the ideal-MHD rate for a significant subset of this range (200 mG $\lesssim B \lesssim 500$ mG). Hall diffusion modifies the structure and growth of these modes for $B \lesssim 10$ mG. When the field is within this limit, a small magnetically dead region develops but it disappears for stronger B. Note that all the solutions that incorporate dust grains peak at a height above the midplane where ambipolar diffusion is locally dominant (e.g. $z/H \sim 4$ for $B = 10$ mG and $a = 1$ μm; see also the middle panel of Fig. 6). This signals that this diffusivity term shapes the structure of these perturbations and explains why their amplitude increase with height. The solutions computed with the small grain population ($a = 0.1$ μm) exhibit, as in the $R = 10$ AU case, an extended dead zone encompassing the region where the magnetic coupling is insufficient to sustain the MRI ($z/H \lesssim 2.5$; see bottom panel of Fig. 4). Solutions are found in this case for $B \lesssim 16$ mG.

The solutions described so far in this section incorporate all diffusion mechanisms (represented by $\eta_{\rm A}$, $\eta_{\rm H}$ and $\eta_{\rm O}$). For comparison, Fig 9 displays how the full $\boldsymbol{\eta}$ modes at 10 AU and including 0.1 μm-sized grains (left column), are modified if only ambipolar diffusion (middle column) and Hall diffusion (right column) are considered. Note that when the field is weak (e.g. the solutions for $B = 1$ and 4

mG), full $\boldsymbol{\eta}$ perturbations grow faster, and are active closer to the midplane, than modes obtained in the ambipolar diffusion limit. This is the result of the contribution of the Hall diffusivity term (e.g. note that the solution in the Hall limit for $B = 1$ mG grows at the ideal-MHD rate). For $B = 10$ mG, the structure of the modes computed with and without the Hall term are fairly similar, as this diffusion mechanism is no longer important at the z where they peak (see bottom panel of Fig. 3). Note also that modes in the Hall limit do not grow for $B > 4$ mG, a result consistent with ambipolar diffusion being dominant at these field strengths (see bottom panel of Fig. 3).

A similar comparison is shown in Fig. 10 for $R = 5$ AU and incorporating the effect of 3 μm-sized dust particles. The Hall term is important here also, as evidenced by the faster growth and more extended unstable zone of the perturbations that include this diffusion mechanism. Ambipolar diffusion strongly influences the structure of the modes for intermediate field strengths (e.g. compare the solutions with $B = 10$ mG and different configurations of the diffusivity tensor) and the perturbations grow in this limit for a reduced range of B in relation to that associated with full $\boldsymbol{\eta}$ (or Hall limit) modes.

The dependence of the growth rate of the most unstable mode ($\nu_{\rm max}$) with the strength of the magnetic field is summarised in Fig. 11 for different assumptions regarding the presence, and radius, of dust grains mixed with the gas. Results are shown for $R = 10$ AU (top panel) and 5 AU (bottom panel). Note that $\nu_{\rm max}$ drops sharply at a characteristic field strength ($B_{\rm max}$), which is a function of both the properties of the grain population and the radial position. The maximum field strength for which perturbations grow in a particular scenario is weaker at larger radii, an effect that is particularly noticeable when no grains are present. This behaviour results from the instability being (generally) damped when the midplane ratio of the Alfvén to sound speed approaches unity (e.g. $v_{\rm A0}/c_{\rm s} \sim 1$; Balbus & Hawley 1991)[2] and the wavelength of the most unstable mode becomes $\sim H$. As the midplane density and temperature decrease with radius, the ratio $v_{\rm A0}/c_{\rm s}$, associated with a particular field strength, increases at larger radii and the perturbations are damped at a weaker field as r increases. Note also that for each radii, the range of field strengths over which unstable modes exist is smaller as the grain size diminishes. This is consistent with the drop in magnetic coupling for a particular field strength as the dust particles are smaller (see Figs. 3 and 4).

Finally, note that at 5 AU and for weak fields ($B \lesssim 5$ mG, bottom panel of Fig. 11) the MRI grows faster when the small grains are considered than it does in the other scenarios. This is because in this case the modes grow high above the midplane, where the magnetic coupling is more favourable, and are completely suppressed at lower z. In the other cases, on the contrary, the perturbations grow over a more extended section of the disc and the comparatively low magnetic coupling closer to the midplane reduces their global growth rate. This effect is not so noticeable at 10 AU by the relatively high magnetic coupling even at $z = 0$ at this radius.

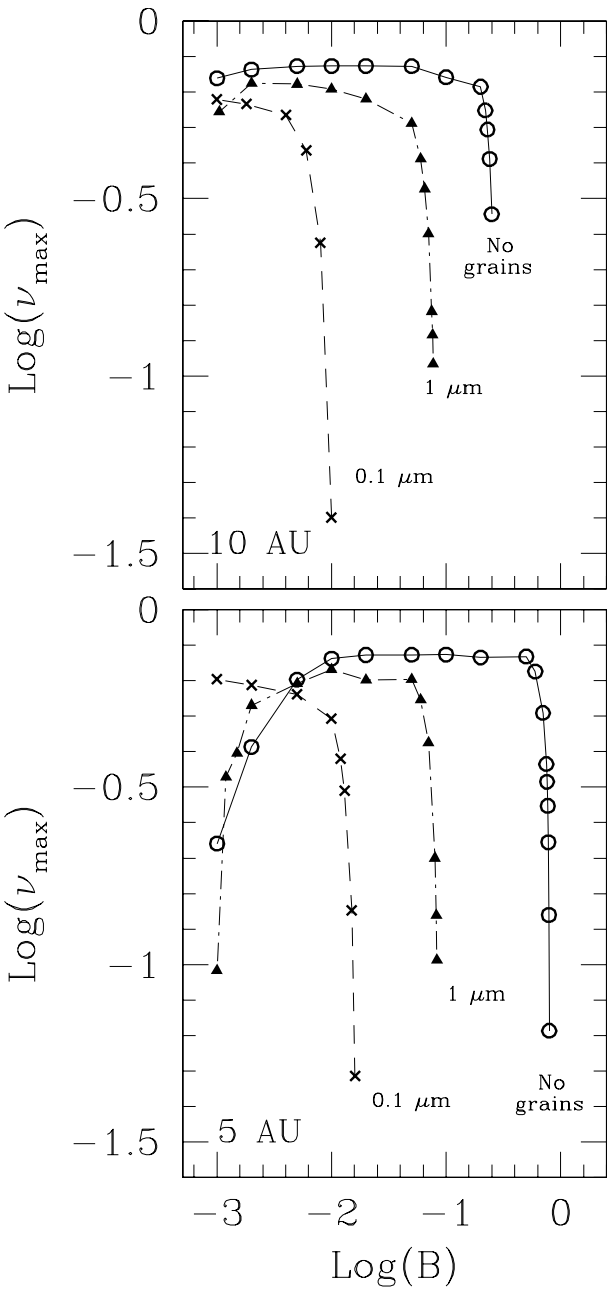

Figure 11. Growth rate of the most unstable MRI modes as a function of the strength of the magnetic field for different assumptions regarding the presence, and size, of dust grains mixed with the gas. Solutions are presented for $R = 10$ AU (top panel) and $R = 5$ AU (bottom panel).

5 DISCUSSION

In this paper we have examined illustrative examples of the impact of dust grains in the magnetic activity of protoplanetary discs and, in particular, in the linear growth and vertical structure of MRI perturbations. Solutions were computed

[2] Note, however, that perturbations computed in the Hall limit have been found to grow for $v_{\rm A0}/c_{\rm s} \lesssim 3$ (SW03) when the magnetic field is counteraligned with the disc angular velocity vector ($\boldsymbol{\Omega}$).

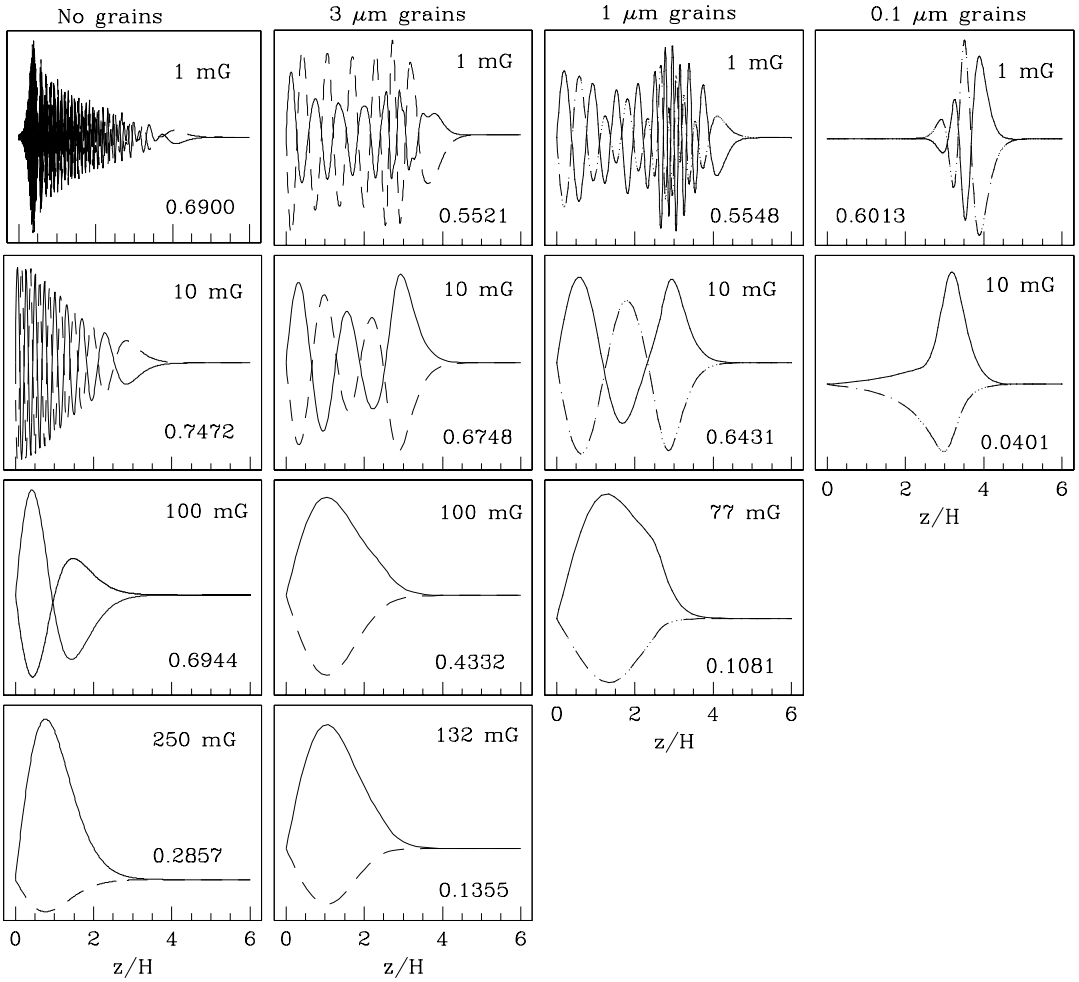

Figure 7. Structure and growth rate of the fastest growing MRI modes for $R = 10$ AU and different choices of the magnetic field strength. The leftmost column shows the perturbations obtained if dust grains have settled, while the remaining ones, from left to right, display results assuming a population of single-sized grains of radius $a = 3$, 1 and 0.1 μm, respectively, are well mixed with the gas. The growth rate is indicated in the lower right corner of each panel. The strength of the field appears in the top right corner. Results are displayed for B spanning from 1 mG, the weakest magnetic field for which unstable modes could be computed, to the maximum strength for which unstable modes were found in each case. Note the reduced wavenumber, growth rate and range of B for which perturbations exist – as well as the extended dead zone – when dust grains are present. When the grains are relatively large (central two columns) Hall diffusion controls the modes, which grow even at the midplane. In contrast, when they are small (right column), the magnetic coupling is too low to sustain the instability for $z/H \lesssim 3$ and ambipolar diffusion controls the perturbations that grow above this height.

for $R = 10$ and 5 AU assuming a single size grain population of radius $a = 0.1$, 1 or 3 μm, and constituting 1 % of the total mass of the gas, is well mixed with the gas phase over the entire vertical extent of the disc. This fraction is independent of height, so we have also assumed that the grains have not sedimented towards the midplane. Our results indicate that the perturbations' wavenumber and growth rate are significantly reduced when grains are present. Furthermore, the magnetically inactive – dead – zone, which was practically non-existent when grains were settled, extends to $z/H \sim 3$ at either radii when 0.1 μm-sized grains are considered. At 10 AU (5 AU), unstable perturbations were found in this case for $B \lesssim 10$ mG (16 mG), a much reduced range compared with the strengths for which they exist when no grains are involved (250 and 795 mG, respectively). This maximum field strength corresponds well to the equipartition field at the height at which the perturbations peak, as expected (e.g. $z/H \approx 3.7$ at 10 AU; see lower right panel of Fig. 7).

These results illustrate the impact of dust particles on the dynamics – and evolution – of low conductivity discs. They can also be used to estimate the maximum magnetic field strength to support magnetic activity at 1 AU. The magnetic coupling at this radius, in a disc including 0.1 μm grains, is too weak below $z/H \sim 3.5$ to allow the field to sufficiently couple with the gas (W07). Assuming that the maximum field strength for the MRI to grow is also of the order of the equipartition field at about this height, we can roughly estimate that the MRI should be active for $B \lesssim 400$ mG at 1 AU. This is a smaller range than the several gauss for which unstable modes exist when dust grains are not present (SW05). However, MRI modes still grow in this case for a wide range of field strengths.

The results just presented were obtained assuming that all grains have the same size and are well mixed with the

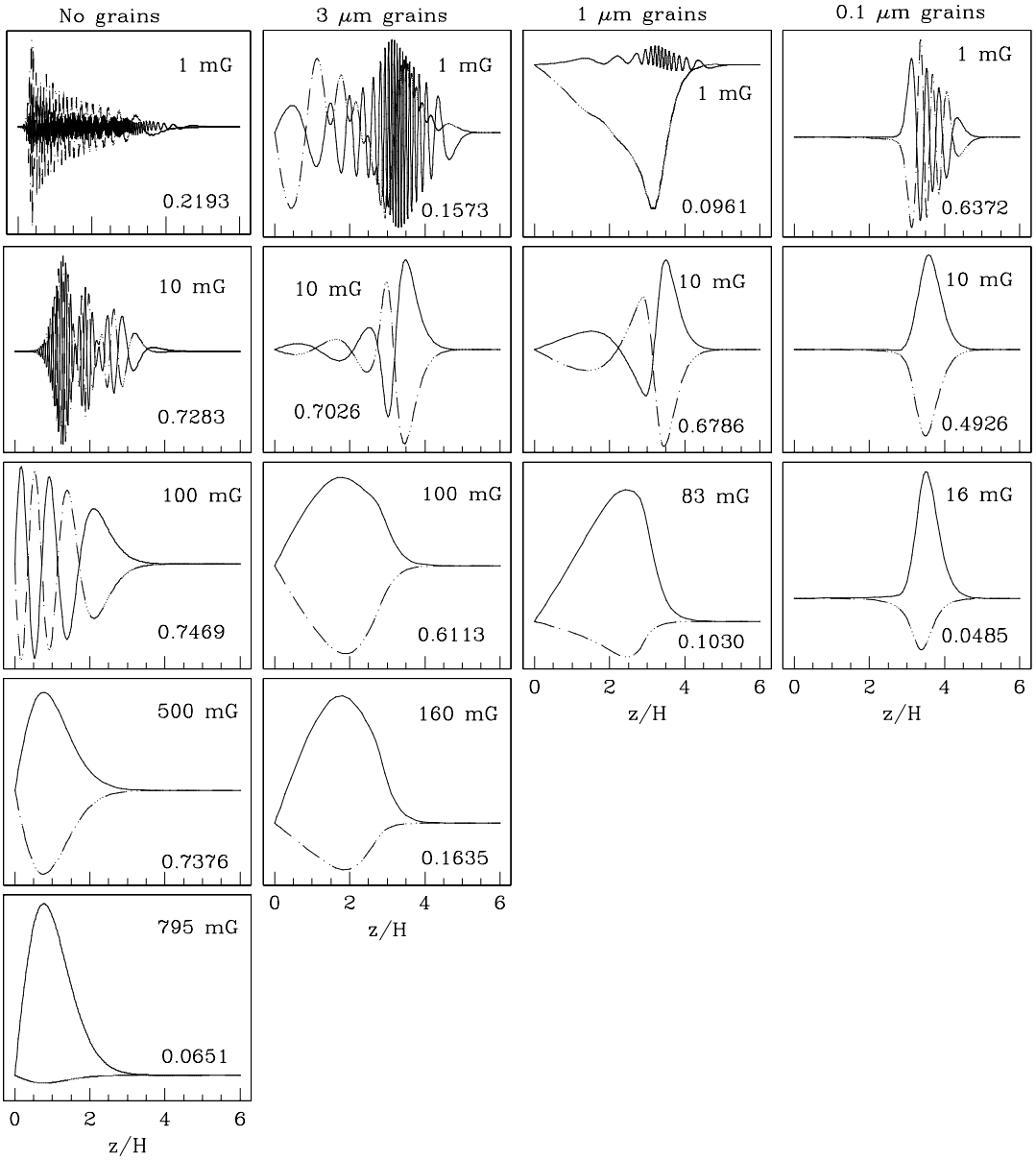

Figure 8. As per Fig. 7 for $R = 5$ AU. At this radius, the solutions that incorporate 3 and 1 μm-sized grains (central two columns) are shaped by ambipolar diffusion, as this mechanism is dominant at the height where they peak (see middle panel of Fig. 6). Note the extended dead zone when the grains are small (right column). In this scenario, severe magnetic diffusivity prevents the magnetic field from coupling to the gas for $z/H \lesssim 2.5$ and ambipolar diffusion dominates at higher z where the MRI grows.

gas at all z. More realistic spatial, and size, distributions must incorporate the effects of dust dynamics and evolution within the disc. Observations of the mid – and far – infrared spectra of discs have provided credible indications that dust properties in discs are indeed different from those of particles in diffuse clouds (e.g. Van Dishoeck 2004, D'Alessio et al. 2006 and references therein). Two aspects of this dust evolution have been clearly identified. First, dust grains coagulate from 0.1 μm to ~ 1 mm particles. Second, (silicate) material becomes crystallised. It is believed that this crystallisation occurs in the disc, given that crystalline silicates are absent from the interstellar medium. Furthermore, the presence of this material at radial locations where the temperature is too low to produce them, suggests significant radial mixing takes place as well (e.g. Van Dishoeck 2004 and references therein). Finally, simulations of dust dynamics and evolution also suggest that in quiescent environments, the grains tend to settle and agglomerate into bigger particles (e.g. Weidenschilling & Cuzzi 1993) and efficiently coagulate and grow icy mantles (Ossenkopf 1993). All these processes modify the surface area of dust grains and impact the recombination rate on their surfaces and the way they drift in response to magnetic stresses. It is also expected that a residual population of small grains would remain (e.g. Nomura et al. 2006) even when the mean grain size maybe relatively large ($a \gtrsim 1\mu$m). This is an important consideration because these small grains tend to carry a significant fraction of the grain charge (S07). The effect of this settling

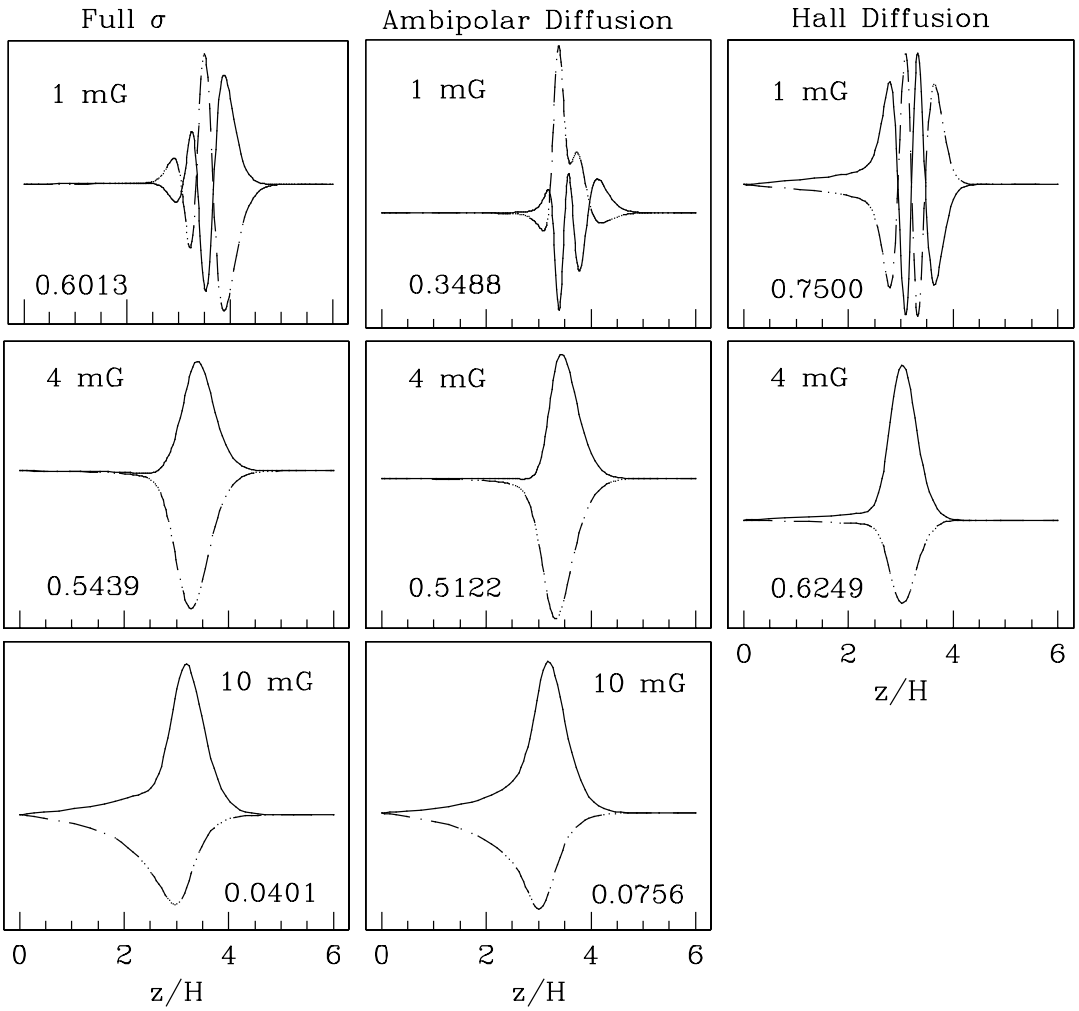

Figure 9. Structure and growth rate of the fastest growing MRI modes as a function of height for $R = 10$ AU and assuming 0.1 μm grains are present. Different configurations of the diffusivity tensor are shown. The left column displays solutions incorporating all $\boldsymbol{\eta}$ components ($\eta_{\rm A}$, $\eta_{\rm H}$ and $\eta_{\rm O}$). The middle and right columns correspond to the ambipolar ($\eta_{\rm H} = 0$) and Hall diffusion ($\eta_{\rm A} = 0$) limits, respectively. We find that for relatively weak fields ($B = 1$ and 4 mG), Hall diffusion causes the perturbations to grow faster and closer to the midplane than solutions in the ambipolar diffusion limit. For $B = 10$ mG, the structure of the modes computed with and without the Hall term are fairly similar, as this diffusion mechanism is no longer important at the z where they peak (see bottom panel of Fig. 3).

in the spectral energy distribution (and optical appearance) of protostellar discs has been investigated in recent studies (e.g. Dullemond & Dominik 2004).

How quickly, and to what height, dust particles are able to settle is an important, and largely unanswered, question. According to Nakagawa, Nakazawa & Hayashi (1981), the mass fraction of $\sim$ 1 - 10 μm grains well mixed with the gas, diminishes from $\sim 10^{-1}$ to 10^{-4} in a timescale of about 2×10^3 to 10^5 years. Moreover, although the timescale for dust grains to sediment all the way to the midplane may exceed the lifetime of the disc, they may be able to settle within a few scaleheights from the midplane in a shorter timescale (Dullemond & Dominik 2004). This is complicated even more by the expectation that the transition between sections were dust grains are well mixed with the gas, and those completely depleted of them, occurs gradually (Dullemond & Dominik 2004).

MHD turbulence may itself be an important factor for the settling of dust particles. It may, in particular, produce sufficient vertical stirring to prevent settling below a certain height (Dullemond & Dominik 2004, Carballido et al. 2005, Turner et al. 2006). However, this is contingent on the disc being able to generate and sustain MHD turbulence in the vertical sections where the dust is present. This is not guaranteed, even if turbulence exists in other regions, as dust grains efficiently reduce the ionisation fraction (and magnetic coupling) of the gas. As a result, the efficiency – and even the viability – of MHD turbulence in the presence of dust grains, is an important topic that merits careful investigation.

6 SUMMARY

We have explored in this paper the linear growth and vertical structure of MRI unstable modes at two representative radii ($R = 5$ and 10 AU) in protoplanetary discs. Dust grains are assumed to be well mixed with the fluid over the entire section of the disc and, for simplicity, are taken to have

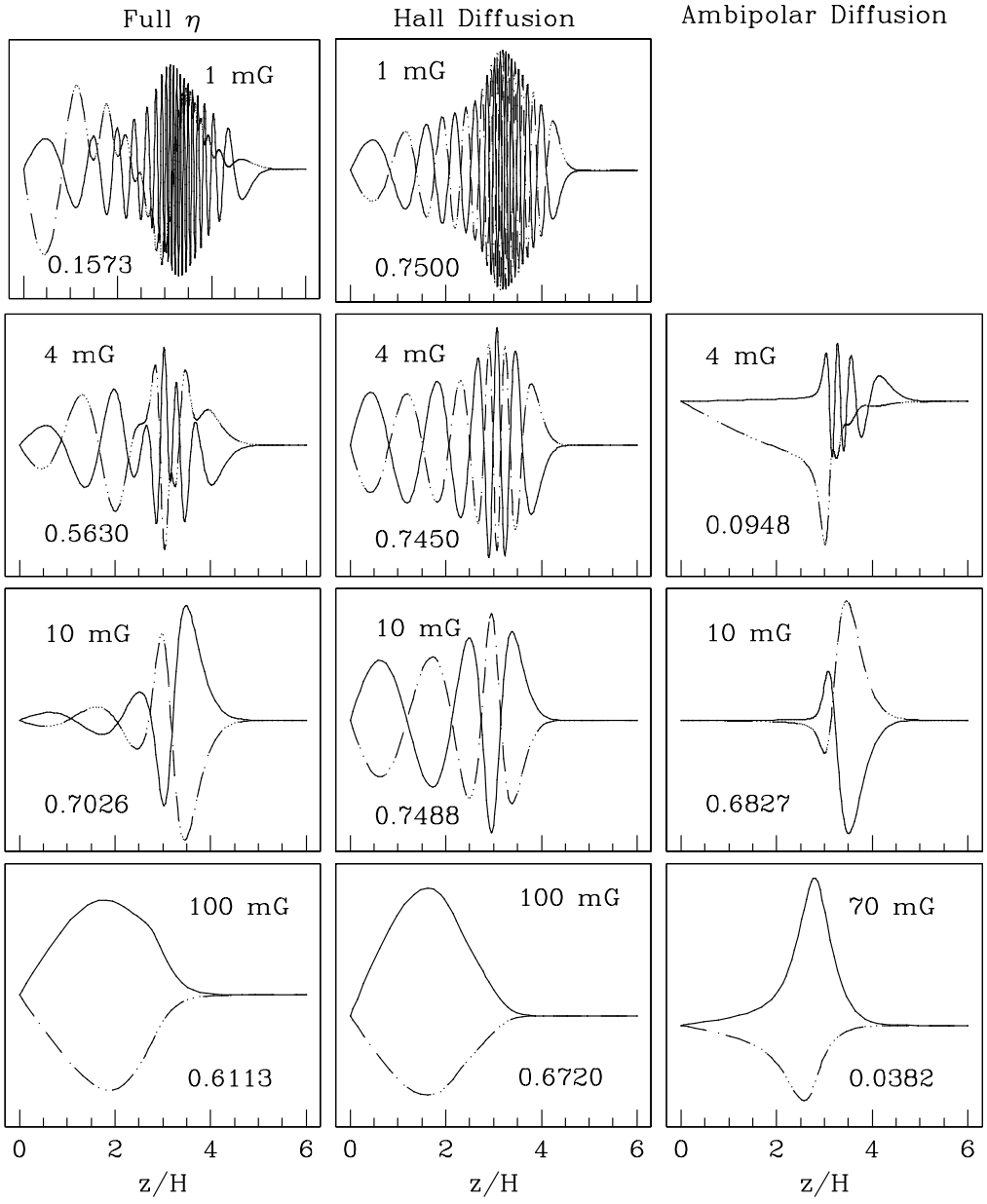

Figure 10. Structure and growth of the fastest growing MRI modes as a function of height at $R = 5$ AU and assuming 3 μm grains are present. The left column shows solutions incorporating all $\boldsymbol{\eta}$ components ($\eta_{\rm A}$, $\eta_{\rm H}$ and $\eta_{\rm O}$). The middle and right columns display the Hall ($\eta_{\rm A} = 0$) and ambipolar diffusion ($\eta_{\rm H} = 0$) limits, respectively. Hall diffusion strongly modifies the structure and growth of unstable modes.

the same radius (a = 3, 1 or 0.1 μm). They constitute a constant fraction (1%) of the total mass of the gas. These solutions are compared with those arrived at assuming that the grains have settled to the midplane of the disc (SW05). We have also explored which disc sections are expected to be magnetically coupled and the dominant diffusion mechanism as a function of height and the strength of the magnetic field, which is initially vertical.

Our models use a minimum-mass solar nebula disc (Hayashi 1981, Hayashi et al. 1985) and incorporate all three diffusion mechanisms between the magnetic field and the neutral gas: Ohmic, Hall and Ambipolar. The diffusivity components are a function of height (as is the density) and are obtained using the method described in W07, to which we refer the reader for details. Essentially, this formalism uses a chemical reaction scheme similar to that of Nishi, Nakano & Umebayashi (1991), but it incorporates higher dust-grain charge states that are likely to occur in discs on account of their larger gas density and temperature in relation to those of molecular clouds. Our calculations also include a realistic ionisation profile, with the main ionising sources being cosmic rays, X-rays and (to a lesser extent) radioactive decay.

Solutions were obtained at the two radii of interest for different grain sizes and configurations of the diffusivity tensor as a function of the magnetic field strength. We refer the reader to SW03 and SW05 for further details of the integra-

tion procedure. The main findings of this study are detailed below.

Magnetic diffusivity

(i) When no grain are present, or they are $\gtrsim 1$ μm in radius, the midplane of the disc remains magnetically coupled for field strengths up to a few gauss at both radii.

(ii) In contrast, when a population of small grains ($a = 0.1\mu$m) is mixed with the gas, the section of the disc below $z/H \sim 2$ ($z/H \sim 2.5$) is magnetically inactive at $R = 10$ AU (5 AU). Only magnetic fields weaker than 25 mG (50 mG) can couple to the gas.

(iii) At 5 AU, Ohmic diffusion dominates for $z/H \lesssim 1.2$ when the field is relatively weak ($B \lesssim$ a few milligauss), irrespective of the properties of the grain population. Conversely, at 10 AU this diffusion term is unimportant in all the scenarios studied here.

(iv) High above the midplane ($z/H \gtrsim 4.5 - 5$, depending on the specific model), ambipolar diffusion is severe and prevents the field from coupling to the gas for all B. This is consistent with previous results by W07.

(v) Hall diffusion is dominant for a wide range of field strengths and grain sizes at both radii (see Figs. 3 and 4).

Magnetorotational instability

(i) The growth rate, wavenumber and range of magnetic field strengths for which unstable modes exist are all drastically diminished when dust grains are present, particularly when they are small ($a \sim 0.1$ μm; see Figs. 7 and 8).

(ii) In all cases that involve dust grains, perturbations that incorporate Hall diffusion grow faster than those obtained under the ambipolar diffusion approximation.

(iii) At 10 AU, unstable MRI modes grow for $B \lesssim 80$ mG (10 mG) when the grain size is 1 μm (0.1 μm), a much reduced range compared with the ~ 250 mG for which they exist when ions and electrons are the only charge carriers (SW05). When the grains are relatively large ($a = 1$ and 3 μm), Hall diffusion controls the structure the modes, which grow even at the midplane. In contrast, when the grains are small ($a = 0.1$ μm), the perturbations grow only for $z/H \gtrsim 3$ and are shaped mainly by ambipolar diffusion.

(iv) At 5 AU, MRI perturbations exist for $B \lesssim 80$ mG (16 mG) when the grains are 1 μm (0.1 μm) in size. For comparison, the upper limit when no grains are present is ~ 800 mG (SW05). These modes are shaped largely by ambipolar diffusion, the dominant mechanism at the height where they peak.

We conclude that in protoplanetary discs, the magnetic field is able to couple to the gas and shear over a wide range of fluid conditions even when small dust grains are well mixed with the gas. Despite the low magnetic coupling, MRI modes grow for an extended range of magnetic field strengths and Hall diffusion largely determines the properties of the perturbations in the inner regions of the disc.

ACKNOWLEDGMENTS

This research has been supported by the Australian Research Council. RS acknowledges partial support from NASA Theoretical Astrophysics Program Grant NNG04G178G.

REFERENCES

Balbus S. A., Hawley J. F., 1991, ApJ, 376, 214
Balbus S. A., Hawley J. F., 1998, Rev. Mod. Phys., 70, 1
Blandford R.D., Payne D.G., 1982, MNRAS, 199, 883 (BP82)
Carballido A., Stone J. M., Pringle J. E., 2005, MNRAS, 358, 1055
Consolmagno G. J., Jokipii J. R., 1978, Moon Planets, 19, 253
Cowling, T. G. 1957, Magnetohydrodynamics (New York: Interscience)
D'Alessio P., Calvet N., Hartmann L., Franco–Hernandez R., Servin H., 2006, ApJ, 638, 314
Dullemond C. P., Dominik C., 2004, A&A, 421, 1075
Fromang S., Terquem C., Balbus S. A., 2002, MNRAS, 329, 18
Gammie C. F., 1996, ApJ, 457, 355
Glassgold A. E., Feigelson E. D., Montmerle T., 2000, in Protostars & Planets IV, ed. V. G. Mannings, A. P. Boss, S. Russell (Tucson: Univ. Arizona Press), p. 429
Glassgold A. E., Najita J., Igea J., 1997, ApJ, 480, 344
Hayashi C., 1981, Prog Theor Phys Supp, 70, 35
Hayashi C., Nakasawa K., Nakagawa Y., 1985, in Protostars & Planets II, ed. D.C. Black, M. S. Mathews (Tucson: Univ. Arizona Press), p. 1100
Igea J., Glassgold A. E., 1999, ApJ, 518, 848
Ilgner M., Nelson R. P., 2006, A&A, 445, 223
Johnson E. T., Goodman J., Menou K., 2006, ApJ, 647, 1413
Königl A., Pudritz R. E., 2000, in Mannings, V. G., Boss, A. P., Russell, S. eds, Protostars & Planets IV. Univ. Arizona Press, Tucson, p. 759
Mathis J. S., Rumpl W., Nordsieck K. H., 1977, ApJ, 217, 425
Matsumura S., Pudritz R. E., 2005, ApJ, 618, L137
Morton D. C., 1974, Astrophys. J., 193, L35
Nakagawa Y., Nakazawa K., Hayashi C., 1981, Icarus, 45, 517
Nakano T., Umebayashi T. 1986, MNRAS, 218, 663
Nishi R., Nakano T., Umebayashi T., 1991, ApJ, 368, 181
Nomura H., Nakagawa Y., 2006, ApJ, 640, 1099
Norman C., Heyvaerts J., 1985, AA, 147, 247
Oppenheimer M., Dalgarno A., 1974, ApJ, 192, 29
Ossenkopf V., 1993, AA, 280, 617
Salmeron R., Wardle M., 2003, MNRAS, 345, 992 (SW03)
Salmeron R., Wardle M., 2005, MNRAS, 361, 45 (SW05)
Sano T., Stone J. M., 2002a, ApJ, 570, 314
Sano T., Miyama S., Umebayashi J., Nakano T., 2000, ApJ, 543, 486
Semenov D., Wiebe D., Henning Th., 2006, ApJ, 647, L57
Spitzer, L. 1978, Physical Processes in the Interstellar Medium (New York: Wiley)
Terquem C., 2003, MNRAS, 341, 1157
Turner N. J., Willacy K., Bryden G., Yorke H. W., 2006, ApJ, 639, 1218
Umebayashi T., Nakano T., 1980, PASJ, 32, 405
Umebayashi T., Nakano T., 1990, MNRAS, 243, 103
Van Dishoeck E. F., 2004, ARA&A, 42, 119
Wardle, M., Königl, A. 1993, ApJ, 410, 218
Wardle M., 1997, in Proc. IAU Colloq. 163, Accretion Phenomena and Related Outflows, ed. D. Wickramasinghe, L. Ferrario, G. Bicknell (San Francisco: ASP), p. 561
Wardle M., 1999, MNRAS, 307, 849 (W99)
Wardle M., 2007, astro-ph/0704.0970
Wardle M., Ng C., 1999, MNRAS, 303, 239

Weidenschilling S. J., Cuzzi J. N., 1993, in Protostars & Planets III, ed. E. H. Levy, J. I. Lunine (Tucson: Univ. Arizona Press), p. 1031

This paper has been typeset from a TEX/ LATEX file prepared by the author.